Liquidus Projections of Bi-Se-Ga and Bi-Se-Te Ternary Systems

PO-HAN LIN, SINN-WEN CHEN, JENN-DONG HWANG, and HSU-SHEN CHU

This study determines the liquidus projections of both Bi-Se-Ga and Bi-Se-Te ternary systems which are constituent ternary systems of promising Bi-Se-Te-Ga thermoelectric materials. Ternary Bi-Se-Ga and Bi-Se-Te alloys are prepared. Their primary solidification phases are experimentally determined, and thermal analysis experiments are carried out. The liquidus projections are determined based on the ternary experimental results and phase diagrams of constituent binary systems. The Bi-Se-Ga system includes seven primary solidification phases, Bi, Ga, GaSe, Ga_2Se_3, Se, Bi_2Se_3, and $(Bi_2)_n(Bi_2Se_3)_m$. In the Bi-Se-Te system, there are five primary solidification phases, Bi, $(Bi_2)_n(Bi_2Te_3)_m$, $Bi_2(Se,Te)_3$, (Se,Te), and $(Bi_2)_n(Bi_2Se_3)_m$. Both the $(Bi_2)_n(Bi_2Te_3)_m$ and $(Bi_2)_n(Bi_2Se_3)_m$ phases are not a single phase, but a collection of series undetermined phases. Large miscibility gaps are observed in the Bi-Se-Ga system. The temperatures of the invariant reactions, Liquid + Bi + GaSe = Ga and Liquid + Ga_2Se_3 = Bi + GaSe, are at 495 K (222 °C) and 533 K (260 °C), respectively.

DOI: 10.1007/s40553-016-0090-0

I. INTRODUCTION

THERMOELECTRIC devices can convert directly between electricity and heat energies. They have attracted tremendous interest especially in applications of waste heat recovery and solid-state cooling.[1–4] Various kinds of thermoelectric materials have been investigated. Bi_2Te_3-based alloys have good thermoelectric properties. P-type $Bi_xSb_{2-x}Te_3$ and N-type $Bi_2Te_{3-x}Se_x$ alloys are the most commonly used commercial thermoelectric materials nowadays.[1–10] Recent studies indicate that the thermoelectric properties of P-type $Bi_xSb_{2-x}Te_3$ and N-type $Bi_2Te_{3-x}Se_x$ alloys can be further enhanced with Ga alloying.[11–14]

Phase diagrams show fundamental information of material systems and are important for assessment of products' reliabilities and selection of proper processing routes. Although Bi_2Te_3-based alloys are the most commonly used thermoelectric materials, only very limited phase diagram information is available for Bi_2Te_3-related material systems.[15–25] This study determines the liquidus projections of Bi-Se-Ga and Bi-Se-Te ternary systems. These two systems are the constituent ternary systems of the Bi-Se-Ga-Te quaternary system, but their liquidus projections have not yet been reported in the literature.

PO-HAN LIN, Ph.D. Student, and SINN-WEN CHEN, Professor, are with Department of Chemical Engineering, National Tsing Hua University, Hsinchu, Taiwan. Contact e-mail: swchen@mx.nthu.edu.tw JENN-DONG HWANG, Division Director, and HSU-SHEN CHU, Research Supervisor, are with the Material & Chemical Research Laboratory, ITRI, Hsinchu, Taiwan.

Manuscript submitted January 6, 2016.
Article published online June 15, 2016

II. EXPERIMENTAL PROCEDURES

Ternary Bi-Se-Ga and Bi-Se-Te and alloys were prepared with pure constituent elements. Pure Bi shots (99.9 at. pct, Admat Midas, U.S.A.), Se plates (99.999 at. pct, Alfa Aesar, U.S.A.), Te shots (99.99 at. pct, Aesar, U.S.A.), and Ga chunks (99.99 at. pct, Alfa Aesar, U.S.A.) with a total weight of about 1 g were weighed and encapsulated in a quartz tube under a 10^{-5} torr. vacuum. The sample capsules were kept at 1273 K (1000 °C) for 2 days for homogenization and then quenched in water. The as-cast alloys were cut into several pieces for examination.

A piece of the as-cast alloy was mounted and examined by Scanning Electron Microscopy (SEM, Hitachi, S-2500, Japan). The primary solidification phases were the first solid phase precipitated from the liquid phase during solidification and were identified based on the as-cast microstructures. Their compositions were determined by Electron Probe Microanalysis (EPMA, JEOL, JXA-8500F, Japan). A piece of the as-cast alloy was ground into powders and analyzed by powder X-ray diffraction (XRD, Scintac, XDS-2000 V/H, U.S.A.) using Cu-Kα as the radiation source.

The univariant lines of the liquidus projection, *i.e.*, the liquidus trough, delineate the boundaries of the different primary solidification phases. Thus, the determined results of primary solidification phases can be used to construct the univariant lines of the liquidus projection. However, the temperature-descending directions of the univariant lines are determined using the results from thermal analysis. Some of the as-cast alloys were thus analyzed using Differential Thermal Analysis (DTA, Perkin Elmer DTA7, U.S.A.). Both heating and cooling experiments were carried out, and the scanning rate was 10 °C/min.

III. RESULTS AND DISCUSSION

A. *Primary Solidification Phases and the Univariant Lines of the Bi-Se-Ga System*

The primary solidification phases along the three sides of a ternary liquidus projection can be determined from its constituent binary phase diagrams. The three binary constituent systems of the Bi-Se-Ga ternary system are Bi-Ga, Ga-Se, and Bi-Se. There is no binary compound in the Bi-Ga system.[26] The Ga-Se system has GaSe and Ga_2Se_3 compounds,[27] and no efforts are made in this study to differentiate the α-Ga_2Se_3 and β-Ga_2Se_3 phases. Both Bi-Ga and Ga-Se have a miscibility gap at the Ga-rich corner. The Bi-Se system is a very complicated system.[28] Except for the well-known Bi_2Se_3 compound, there are numerous undetermined compounds between the Bi and Bi_2Se_3 phases. They are grouped together and referred to as the $(Bi_2)_n(Bi_2Se_3)_m$ compound,[29] as shown in Figure 1(a). Based on these three binary phase diagrams, the primary solidification phases along the three sides of the ternary Bi-Se-Ga liquidus projection are Bi, Ga, GaSe, Ga_2Se_3, Se, Bi_2Se_3, and $(Bi_2)_n(Bi_2Se_3)_m$. It should be re-mentioned that the $(Bi_2)_n(Bi_2Se_3)_m$ compound is not a single phase but a series of compounds.

Thirty-eight ternary Bi-Se-Ga alloys were prepared to determine liquidus projection. Their nominal compositions are listed in Table I and shown in Figure 1(c). Figure 1(d) shows a close-up image of the liquidus projection at the Ga-rich corner. Figure 2(a) shows a BEI (Backscattered Electron Imaging) micrograph of the as-solidified alloy #1 (Bi-5.0 at. pct Se-45.0 at. pct Ga). The micrograph with a higher magnification is overlaid on the upper left corner. Based on the microstructure as shown in Figure 2(a), the bright phase is the first solidification phase. Its composition is Bi-0.2 at. pct Se-0.1 at. pct Ga and is the Bi phase. Figure 2(b) shows the XRD diffractogram. Diffraction peaks of Bi are observed. The XRD results are consistent with EPMA determinations, and the primary solidification phase of alloy #1 is Bi. Similar results are observed for alloys #2 (Bi-2.0 at. pct Se-28.0 at. pct Ga), #3 (Bi-2.0 at. pct Se-48.0 at. pct Ga), #6 (Bi-5.0 at. pct Se-25.0 at. pct Ga), and #9 (Bi-5.0 at. pct Se-15.0 at. pct Ga), and all their primary solidification phases are the Bi phase.

As shown in Figures 2(a) and (b), in addition to the Bi phase, other phases are formed during the later stages of solidification. For example, GaSe and Ga phases are observed in the as-solidified alloy #1. Solidification of multicomponent alloys is complicated and detailed analysis of all the solidified phases requires extensive efforts. Furthermore, the secondary and tertiary phases are not the main interests of this study. Thus, only the primary solidification phases were identified and examined.

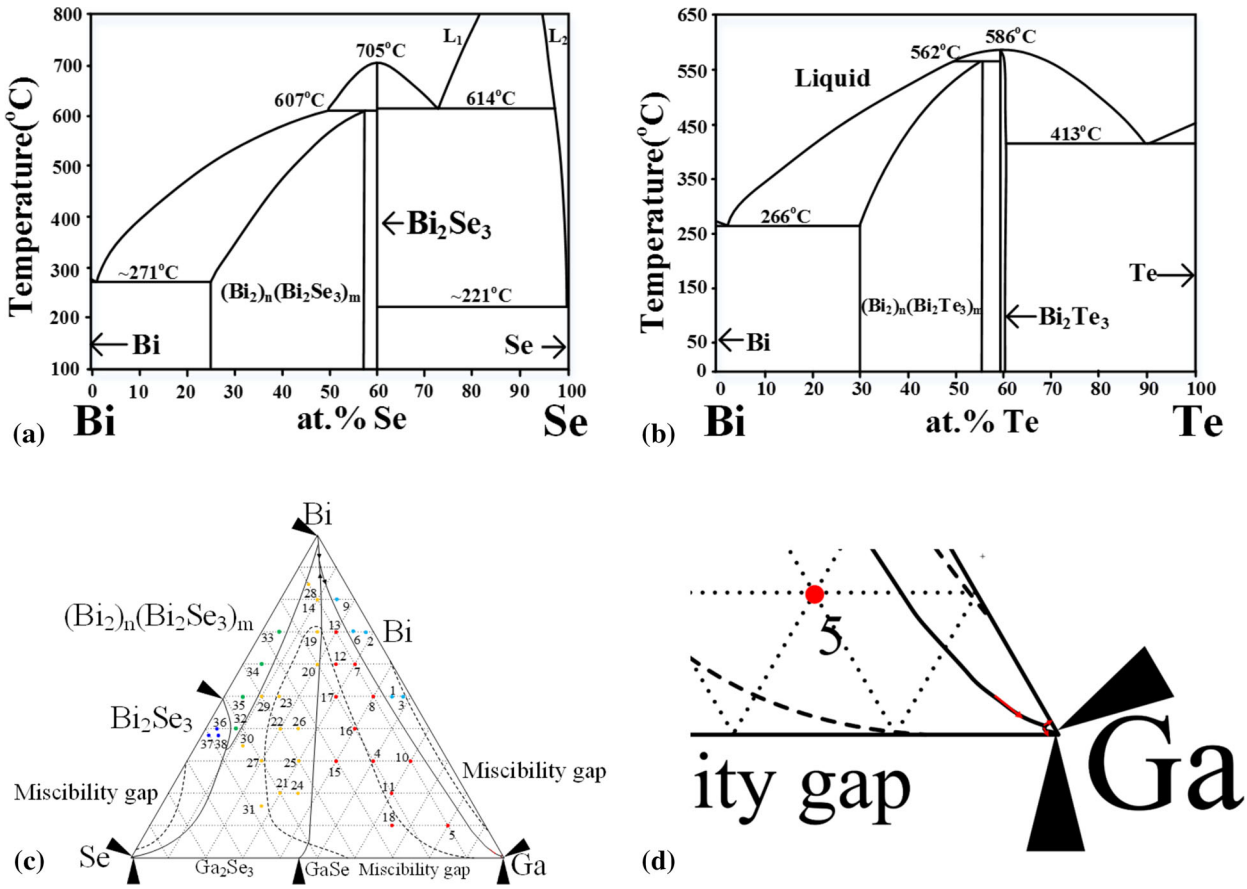

Fig. 1—(*a*) Bi-Se phase diagram, (*b*) Bi-Te phase diagram, (*c*) compositions of ternary Bi-Se-Ga alloys examined in this study superimposed on the Bi-Se-Ga liquidus projection, and (*d*) a close-up image of Ga-rich corner.

Table I. Primary Solidification Phases of Bi-Se-Ga Alloys

Nominal Composition (at. pct)				
No.	Bi (at. pct)	Se (at. pct)	Ga (at. pct)	Primary phase
#1	50.0	5.0	45.0	Bi
#2	70.0	2.0	28.0	Bi
#3	50.0	2.0	48.0	Bi
#4	30.0	20.0	50.0	GaSe
#5	10.0	10.0	80.0	GaSe
#6	70.0	5.0	25.0	Bi
#7	60.0	10.0	30.0	GaSe
#8	50.0	10.0	40.0	GaSe
#9	80.0	5.0	15.0	Bi
#10	30.0	10.0	60.0	GaSe
#11	20.0	20.0	60.0	GaSe
#12	60.0	15.0	25.0	GaSe
#13	70.0	10.0	20.0	GaSe
#14	80.0	10.0	10.0	Ga_2Se_3
#15	30.0	30.0	40.0	GaSe
#16	40.0	20.0	40.0	GaSe
#17	50.0	20.0	30.0	GaSe
#18	10.0	25.0	65.0	GaSe
#19	70.0	15.0	15.0	Ga_2Se_3
#20	60.0	20.0	20.0	Ga_2Se_3
#21	20.0	50.0	30.0	Ga_2Se_3
#22	40.0	40.0	20.0	Ga_2Se_3
#23	50.0	35.0	15.0	Ga_2Se_3
#24	20.0	45.0	35.0	Ga_2Se_3
#25	30.0	40.0	30.0	Ga_2Se_3
#26	40.0	35.0	25.0	Ga_2Se_3
#27	30.0	50.0	20.0	Ga_2Se_3
#28	85.0	10.0	5.0	Ga_2Se_3
#29	50.0	40.0	10.0	Ga_2Se_3
#30	35.0	52.0	13.0	Ga_2Se_3
#31	15.0	58.0	27.0	Ga_2Se_3
#32	40.0	52.0	8.0	$(Bi_2)_n(Bi_2Se_3)_m$
#33	70.0	25.0	5.0	$(Bi_2)_n(Bi_2Se_3)_m$
#34	60.0	35.0	5.0	$(Bi_2)_n(Bi_2Se_3)_m$
#35	50.0	45.0	5.0	$(Bi_2)_n(Bi_2Se_3)_m$
#36	40.0	57.0	3.0	Bi_2Se_3
#37	38.0	60.0	2.0	Bi_2Se_3
#38	38.0	58.0	4.0	Bi_2Se_3

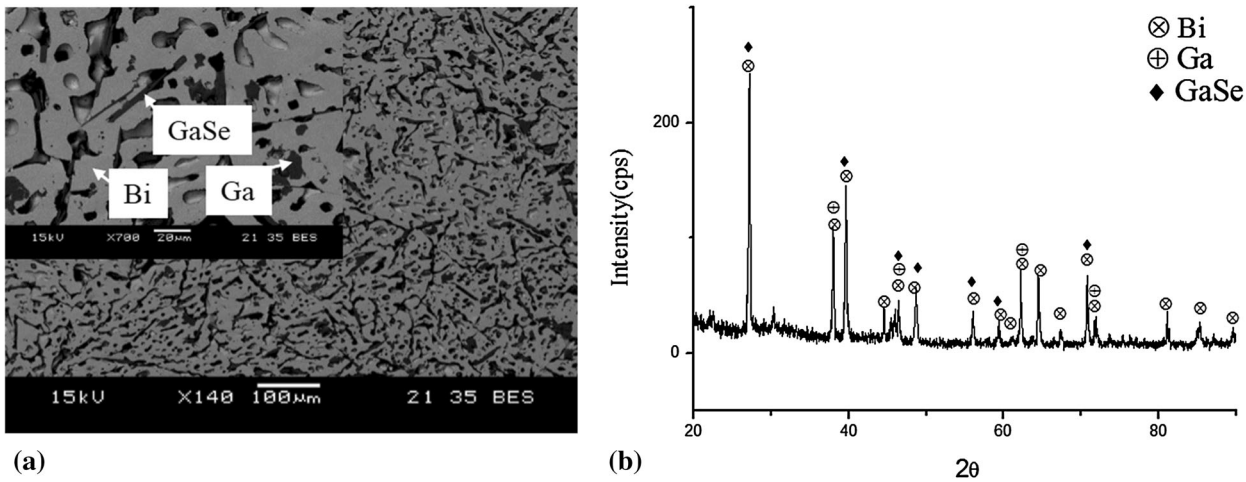

Fig. 2—(*a*) BEI micrograph of the as-solidified alloy #1 (Bi-5.0 at. pct Se-45.0 at. pct Ga) displaying Bi as its primary solidification phase and (*b*) XRD diffractogram of the as-solidified alloy #1.

The BEI micrograph of alloy #4 (Bi-20.0 at. pct Se-50.0 at. pct Ga) is shown in Figure 3(a). The primary solidification phase is the dark dendritic phase with a composition of Bi-47.7 at. pct Se-50.7 at. pct Ga. Figure 3(b) shows its X-ray diffractogram. According to the EPMA and XRD results, the primary solidification phase of alloy #4 is the GaSe phase. Similar results are observed for alloys #5 (Bi-10.0 at. pct Se-80.0 at. pct Ga), #7 (Bi-10.0 at. pct. Se-30.0 at. pct Ga), #8 (Bi-10.0 at. pct Se-40.0 at. pct Ga), #10 (Bi-10.0 at. pct Se-60.0 at. pct Ga), #11 (Bi-20.0 at. pct Se- 60.0 at. pct Ga), #12 (Bi-15.0 at. pct Se-25.0 at. pct Ga), and #13(Bi-10.0 at. pct Se-20.0 at. pct Ga), and all their primary solidification phases are the GaSe phase.

An unusual microstructure is observed for the as-cast alloy #15 (Bi-30.0 at. pct Se-40.0 at. pct Ga) as shown in Figure 4(a). Clearly there are two different regions. This microstructure indicates that alloy #15 is inside the miscibility gap which has two immiscible liquids at elevated temperatures. The as-solidified microstructures of the alloys in the miscibility gap have been investigated.[31] When the volume fractions of the two liquid phases are almost equal, an irregular microstructure can be observed.[31] Both the primary solidification phases of the bright upper half and the dark lower half are the dark stripe-like GaSe phase. Their compositions are both about Bi-48.6 at. pct Se-50.1 at. pct Ga. The XRD result, as shown in Figure 4(b), is in agreement with the microstructural analysis and the primary solidification phase is GaSe phase. Alloys #16, #17, and #18 also have similar metallographic results and their primary solidification phases are the GaSe phase. As shown in Figure 1(c), very large miscibility gaps are observed in the Bi-Se-Ga system.

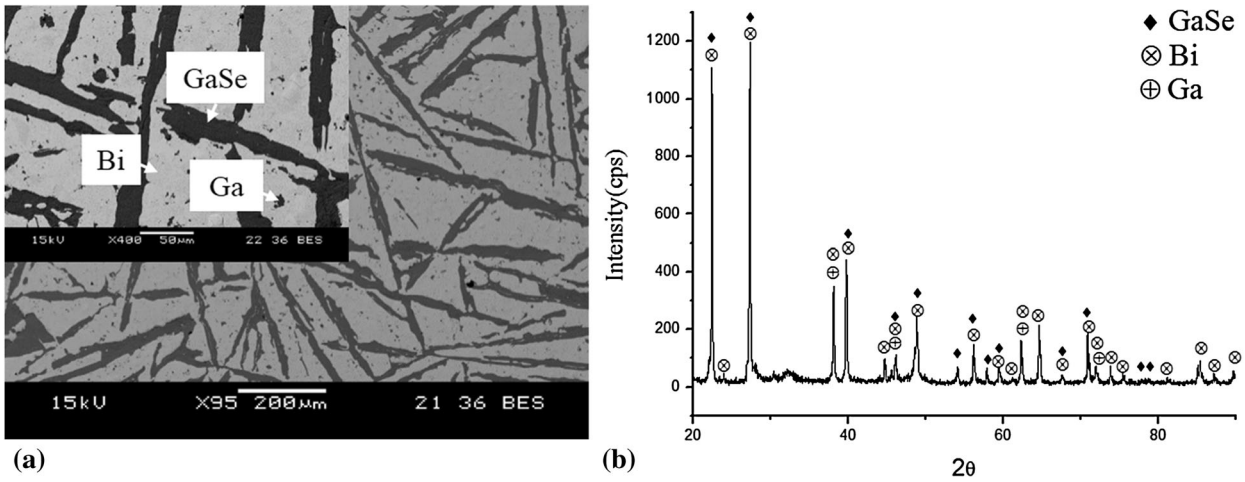

Fig. 3—(*a*) BEI micrograph of the as-solidified alloy #4 (Bi-20.0 at. pct Se-50.0 at. pct Ga) displaying GaSe as its primary solidification phase and (*b*) XRD diffractogram of the as-solidified alloy #4.

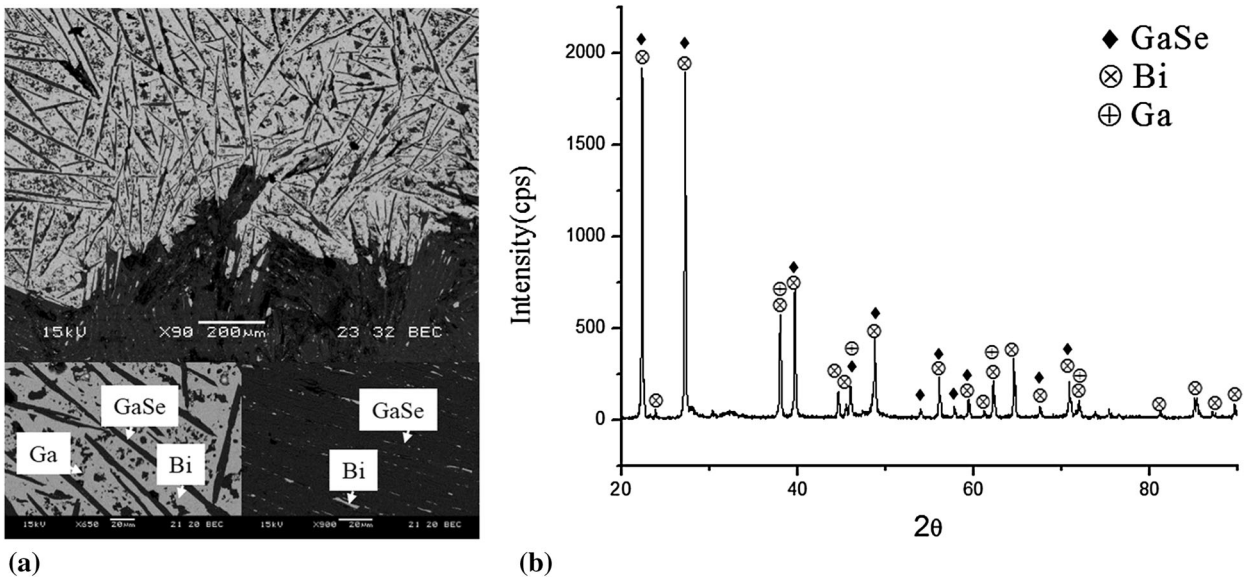

Fig. 4—(*a*) BEI micrograph of the as-solidified alloy #15 (Bi-30.0 at. pct Se-40.0 at. pct Ga) displaying GaSe as its primary solidification phase and (*b*) XRD diffractogram of the as-solidified alloy #15.

Figures 5(a) and (b) and 6(a) and (b) show the BEI micrographs and the X-ray diffractograms of alloys #21 (Bi-50.0 at. pct Se-30.0 at. pct Ga) and #38 (Bi-58.0 at. pct Se-4.0 at. pct Ga), respectively. Following similar analytical procedures, their primary solidification phases are Ga_2Se_3 and Bi_2Se_3, respectively. The primary solidification phase results are summarized in Table I. It should be noted that, as mentioned above, there are many undetermined binary compounds in Bi-Se binary system, and they are grouped together as $(Bi_2)_n(Bi_2Se_3)_m$. Due to their complex nature, this region has not been experimentally examined in this study. Furthermore, a significant mass loss was encountered for the alloys with Se compositions higher than 60 at. pct, and thus there were no reliable experimental data at the Se-rich corner.

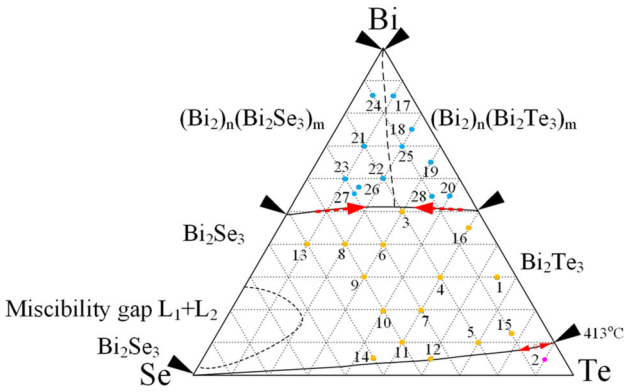

Fig. 7—Compositions of ternary Bi-Se-Te alloys examined in this study superimposed on the Bi-Se-Te liquidus projection.

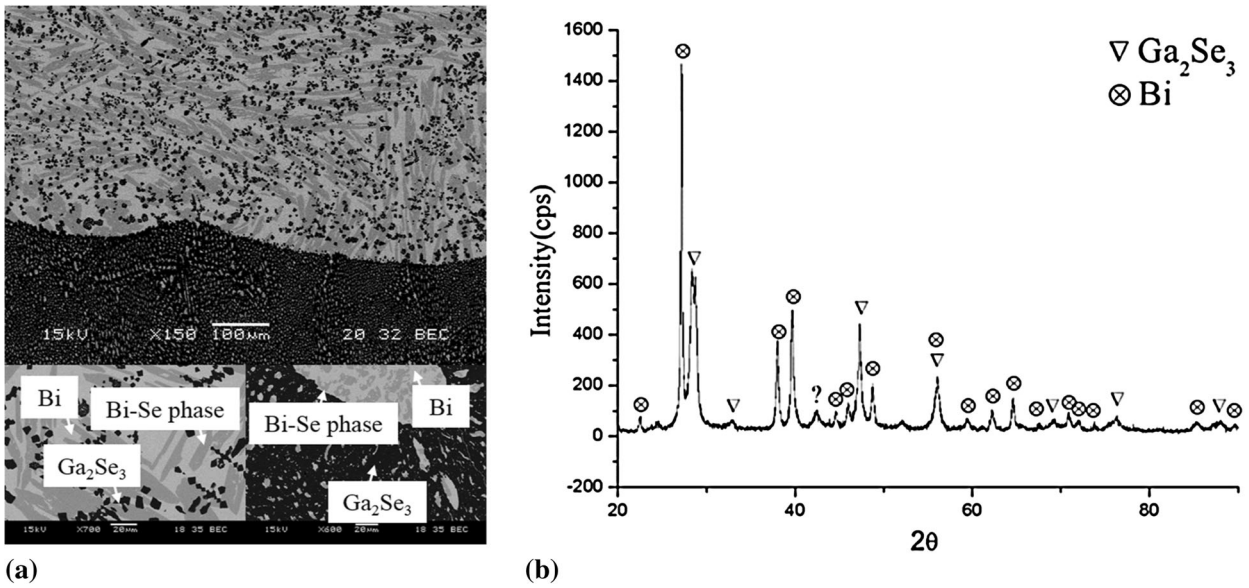

Fig. 5—(*a*) BEI micrograph of the as-solidified alloy #21 (Bi-50.0 at. pct Se-30.0 at. pct Ga) displaying Ga_2Se_3 as its primary solidification phase and (*b*) XRD diffractogram of the as-solidified alloy #21.

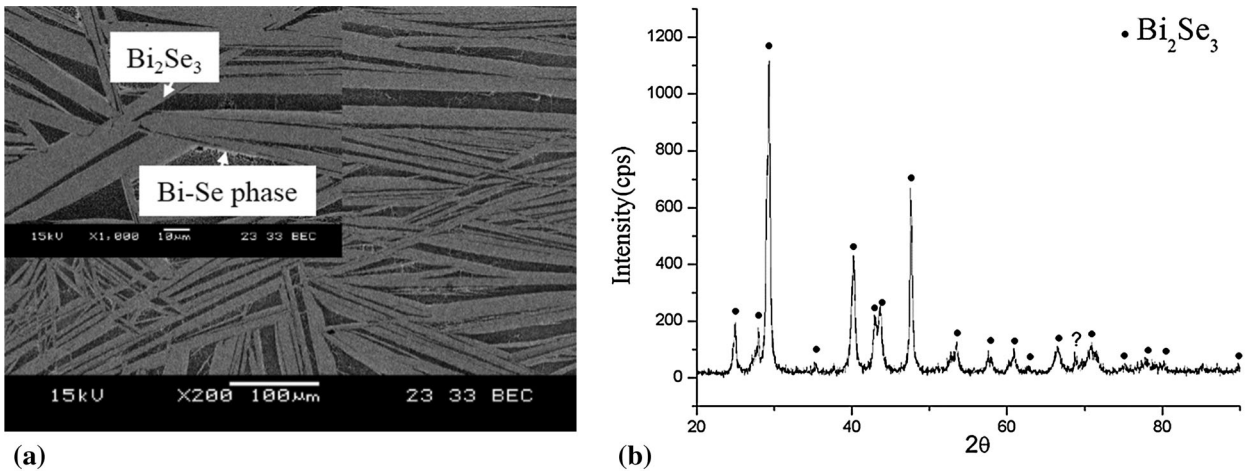

Fig. 6—(*a*) BEI micrograph of the as-solidified alloy #38 (Bi-58.0 at. pct Se-4.0 at. pct Ga) displaying Bi_2Se_3 as its primary solidification phase and (*b*) XRD diffractogram of the as-solidified alloy #38.

The Bi_2Se_3-Ga_2Se_3 isoplethal section was determined by Eholié and Flahaut[24] and Rustamov and Seidova.[25] The results are similar. The Bi_2Se_3-Ga_2Se_3 isoplethal section is a pseudobinary system with a eutectic reaction and only limited solubilities. The BiSe-Ga_2Se_3 isoplethal section was determined by Eholié and Flahaut.[24] A ternary compound, $BiGa_2Se_4$, was found. Eholié and Flahaut[24] also determined the $BiGa_2Se_4$-Bi_2Se_3 and Bi-GaSe isoplethal sections. However, no primary solidification phase region of the $BiGa_2Se_4$ compound has been observed. The experimentally determined results of primary solidification phases are summarized in Table I, and the information obtained from binary phase diagrams and the literatures are then put together to construct the univariant lines of Bi-Se-Ga liquidus projection, as shown in Figures 1(c) and (d). The phase boundaries which are not experimentally confirmed are marked with dashed lines. The primary solidification phase regions are Bi, Ga, GaSe, Ga_2Se_3, Se, Bi_2Se_3, and $(Bi_2)_n(Bi_2Se_3)_m$, and the GaSe and Ga_2Se_3 have the largest compositional regimes. Since $(Bi_2)_n(Bi_2Se_3)_m$ is not a single phase, there are seven or more primary solidification phases in the Bi-Se-Ga system.

Table II. Primary Solidification Phases of Bi-Se-Te Alloys

Nominal Composition (at. pct)				
No.	Bi (at. pct)	Se (at. pct)	Te (at. pct)	Primary phase
#1	30.0	5.0	65.0	$Bi_2(Se,Te)_3$
#2	5.0	5.0	90.0	(Se,Te)
#3	50.0	20.0	30.0	$Bi_2(Se,Te)_3$
#4	30.0	20.0	50.0	$Bi_2(Se,Te)_3$
#5	10.0	20.0	70.0	$Bi_2(Se,Te)_3$
#6	40.0	30.0	30.0	$Bi_2(Se,Te)_3$
#7	20.0	30.0	50.0	$Bi_2(Se,Te)_3$
#8	40.0	40.0	20.0	$Bi_2(Se,Te)_3$
#9	30.0	40.0	30.0	$Bi_2(Se,Te)_3$
#10	20.0	40.0	40.0	$Bi_2(Se,Te)_3$
#11	10.0	40.0	50.0	$Bi_2(Se,Te)_3$
#12	5.0	35.0	60.0	$Bi_2(Se,Te)_3$
#13	40.0	50.0	10.0	$Bi_2(Se,Te)_3$
#14	5.0	50.0	45.0	$Bi_2(Se,Te)_3$
#15	13.0	10.0	77.0	$Bi_2(Se,Te)_3$
#16	45.0	5.0	50.0	$Bi_2(Se,Te)_3$
#17	85.0	5.0	10.0	uncertain phase
#18	75.0	5.0	20.0	uncertain phase
#19	65.0	5.0	30.0	uncertain phase
#20	55.0	5.0	40.0	uncertain phase
#21	70.0	20.0	10.0	uncertain phase
#22	60.0	20.0	20.0	uncertain phase
#23	60.0	30.0	10.0	uncertain phase
#24	85.0	10.0	5.0	uncertain phase
#25	70.0	10.0	20.0	uncertain phase
#26	57.1	28.6	14.3	uncertain phase
#27	55.0	30.0	15.0	uncertain phase
#28	55.0	10.0	35.0	uncertain phase

B. *Primary Solidification Phases and the Univariant Lines of the Bi-Se-Te System*

The three binary constituent systems of the Bi-Se-Te ternary system are Bi-Se, Se-Te, and Bi-Te. Se-Te is an isomorphous system.[32] Bi-Te[30] is also a very complicated system. Similar to the Bi-Se system,[28] except for the Bi_2Te_3 compound, there are numerous undetermined compounds between Bi and Bi_2Te_3. These compounds are grouped together and referred as the $(Bi_2)_n(Bi_2Te_3)_m$ compound,[33] as shown in Figure 1(b). The Bi_2Se_3-Bi_2Te_3 isoplethal section was determined.[20–22] Bankina and Abrikosov[21] and McHugh and Tiller[22] reported a completely mixed solid phase, but Dumas *et al.*[23] reported differently. A recent study by Bounanani *et al.*[20] proposed that the two phases are completely mixed at higher temperatures and a miscibility gap exists at lower temperatures, and the primary solidification phase is thus $Bi_2(Se,Te)_3$. Unlike the Bi-Se-Ga system, no ternary compounds have been reported in this Bi-Se-Te system. Based on these results, the primary solidification phases are Bi, $(Bi_2)_n(Bi_2Se_3)_m$, $Bi_2(Se,Te)_3$, (Se,Te), and $(Bi_2)_n(Bi_2Te_3)_m$. As shown in Figure 7 and

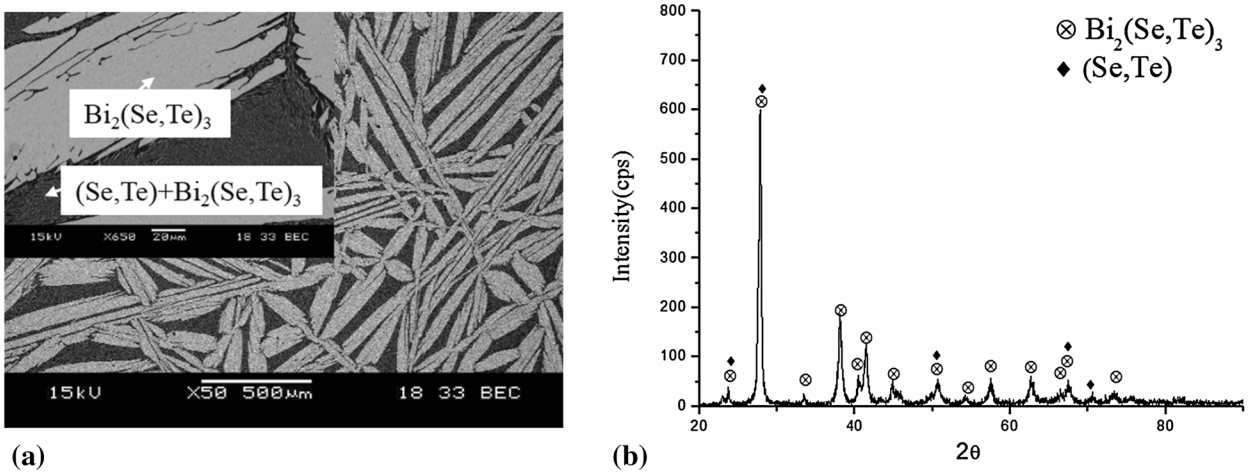

Fig. 8—(*a*) BEI micrograph of the as-solidified alloy #1 (Bi-5.0 at. pct Se-65.0 at. pct Te) displaying $Bi_2(Se,Te)_3$ as its primary solidification phase and (*b*) XRD diffractogram of the as-solidified alloy #1.

Table II, twenty-eight alloys were prepared for the determination of Bi-Se-Te liquidus projection.

Figure 8(a) shows a BEI micrograph of the as-solidified alloy #1 (Bi-5.0 at. pct Se-65.0 at. pct Te), and a close-up micrograph is shown in the upper left corner. The bright dendritic phase is the primary solidification phase. Its composition is Bi-5.6 at. pct Se-54.1 at. pct Te. According to its composition, it is the $Bi_2(Se,Te)_3$ phase which is a continuous solid solution phase formed by Bi_2Se_3 and Bi_2Te_3 phases.[20–23] As shown in Figure 8(a), the dark region is a multiphase region. During the solidification process, with the precipitate of the $Bi_2(Se,Te)_3$ phase, the composition of the remaining liquid moves toward the Se-Te side and away from the Bi-rich corner since the $Bi_2(Se,Te)_3$ phase has higher Bi than its nominal composition. The dark region could have the $Bi_2(Se,Te)_3$ and (Se,Te) phases.

Figure 8(b) shows the powder X-ray diffractogram of the as-solidified alloy #1. The diffraction peaks of the $Bi_2(Se,Te)_3$ and (Se,Te) phases are identified. Alloy #15 (Bi-10.0 at. pct Se-77.0 at. pct Te) also exhibits a similar metallographic result; the composition of the bright primary solidification phase is Bi-25.3 at. pct Se-33.8 at. pct Te, which could indicate a $Bi_2(Se,Te)_3$ phase with higher Se. Because the atomic radius of selenium is smaller than that of tellurium, the diffraction peaks shift to the large angle when the $Bi_2(Se,Te)_3$ phase has higher selenium, as shown in Figure 9. Similar results are observed for alloys #3-#16 where the primary solidification phases are the $Bi_2(Se,Te)_3$.

Figures 10(a) and (b) and 11 show BEI micrographs and XRD diffractograms of alloy #2 (Bi-5.0 at. pct Se-90.0 at. pct Te) and #20 (Bi-5.0 at. pct Se-40.0 at. pct Te). Following similar analytical procedures, their primary solidification phases are determined to be (Se,Te) and $(Bi_2)_n(Bi_2Te_3)_m$ phases, respectively. These results are summarized in Table II, and the related phase diagram information is put together to construct the Bi-Se-Te liquidus projection as shown in Figure 7. The phase boundaries which are not experimentally confirmed are marked with dashed lines. The primary solidification phases are Bi, $(Bi_2)_n(Bi_2Se_3)_m$, $Bi_2(Se,Te)_3$, (Se, Te), and $(Bi_2)_n(Bi_2Te_3)_m$. $Bi_2(Se,Te)_3$ has the largest compositional regime. Since both $(Bi_2)_n(Bi_2Se_3)_m$ and $(Bi_2)_n(Bi_2Te_3)_m$ are not single phases, the Bi-Se-Te system has five or more primary solidification phases.

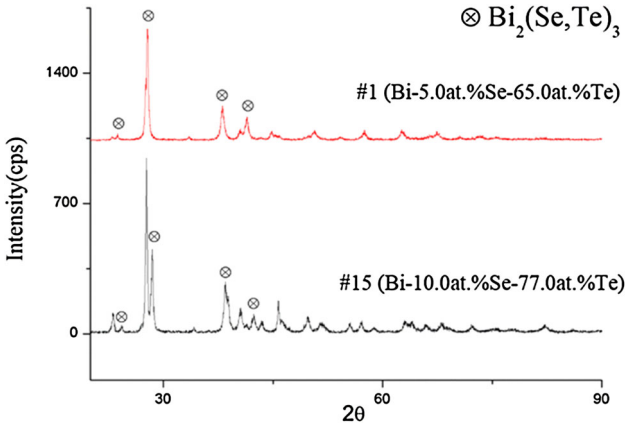

Fig. 9—Peak shift in relation to selenium solubility.

C. *Temperature-Descending Directions of Univariant Lines and Invariant Reaction Temperatures*

In the Bi-Se-Ga system, there are univariant lines between $Bi/(Bi_2)_n(Bi_2Se_3)_m$, Bi/Ga_2Se_3, Bi/GaSe, Bi/Ga, Ga/GaSe, $GaSe/Ga_2Se_3$, Se/Ga_2Se_3, Se/Bi_2Se_3, Bi_2Se_3/Ga_2Se_3, $Bi_2Se_3/(Bi_2)_n(Bi_2Se_3)_m$, and $Ga_2Se_3/(Bi_2)_n(Bi_2Se_3)_m$. The temperature-descending directions are determined based on the thermal analysis results, solidification sequence of phases, and the mass balance requirement.[32–35] Figure 12(a) shows the DTA cooling curve of alloy #11 (Bi-20.0 at. pct Se-60.0 at. pct Ga). Three reactions are observed and are at 529 K, 475 K, and 469 K (256 °C, 202 °C, and 196 °C). The first reaction is the precipitation of the primary solidification phase, GaSe. With the formation of the GaSe phase, the

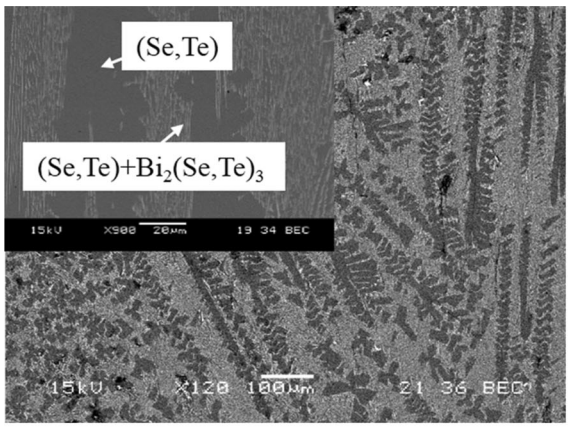

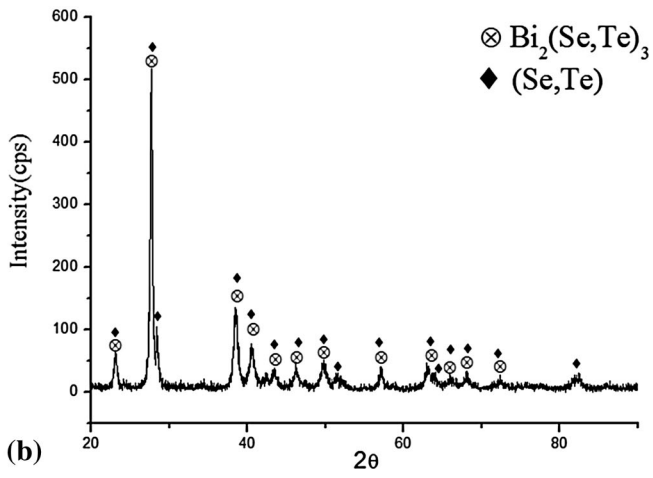

Fig. 10—(*a*) BEI micrograph of the as-solidified alloy #2 (Bi-5.0 at. pct Se-90.0 at. pct Te) displaying (Se,Te) as its primary solidification phase and (*b*) XRD diffractogram of the as-solidified alloy #2.

composition of the remaining liquid moves away from GaSe and intersects with the Bi/GaSe univariant line due to the requirement of mass balance. The second peak is thus caused by the monovariant reaction, i.e., the Bi phase and GaSe phase solidified together. With the formation of both Bi and GaSe, the remaining liquid moves toward the Ga corner following the mass balance requirement. The third reaction peak is caused by the invariant reaction, Liquid + Bi + GaSe = Ga. The temperature-descending direction of the Bi/GaSe univariant line thus moves from the Bi side toward the Ga Side. The solidified phases and their solidification sequence are confirmed by the solidified microstructure as shown in Figure 12(b). Following similar procedures, the temperature-descending directions of the Bi/Ga_2Se_3 and GaSe/Ga_2Se_3 are determined as shown in Figure 1(c).

Although the reaction peaks are usually more noticeable in the cooling curves, the undercooling effect is usually significant, and the reaction temperatures determined from the heating curves are more reliable.[32–35] The invariant reaction temperature, Liquid + Bi + GaSe = Ga, determined from the heating curve is at 495 K (222 °C) and an undercooling of about 26 °C is observed. Following similar procedures, the reaction temperature of the invariant reaction, Liquid + Ga_2Se_3 = GaSe + Bi, is determined to be at 533 K (260 °C), as shown in Table III.

In the Bi-Se-Te system, there are univariant lines between Bi/$(Bi_2)_n(Bi_2Se_3)_m$, Bi/$(Bi_2)_n(Bi_2Te_3)_m$, $(Bi_2)_n(Bi_2Se_3)_m$/$(Bi_2)_n(Bi_2Te_3)_m$, $(Bi_2)_n(Bi_2Se_3)_m$/$Bi_2(Se,Te)_3$, $Bi_2(Se,Te)_3$/ $(Bi_2)_n(Bi_2Te_3)_m$, and $Bi_2(Se,Te)_3$/(Se,Te). Figure 13(a) shows the DTA cooling curve of alloy #15 (Bi-10.0 at. pct Se-77.0 at. pct Te) at a 10°C/minute scanning rate, and two peaks are observed. Based on the liquidus projection shown in Figure 7 and the microstructure shown in Figure 13(b), it is concluded that the first peak at 731 K (458 °C) is caused by the solidification of the $Bi_2(Se,Te)_3$ phase and the second peak at 666 K (393 °C) results from the univariant reaction, *i.e.*, coprecipitation of the $Bi_2(Se,Te)_3$ and (Se,Te) phases. As mentioned above, a significant undercooling is observed in the cooling curve, and the reaction temperatures should be determined from the heating curves. The univariant reaction temperature of alloy #15 is at 687 K (414 °C) as shown in Figure 14(c). Following similar procedures, the univariant reaction temperature of alloy #5 (Bi-20.0 at. pct Se-70.0 at. pct Te) is determined to be 410 K (407 °C), as shown in Figure 14(a). The results indicate that the temperature-descending direction along the $Bi_2(Se,Te)_3$/(Se,Te) univariant line moves toward the Se side and is denoted with an arrow. Figure 14(b) shows the DTA heating curve of alloy #2 (Bi-5.0 at. pct Se-90.0 at. pct Te), and the univariant reaction temperature is at 694 K (421 °C). The $Bi_2(Se,Te)_3$/(Se,Te) univariant line starts along the Bi-Te binary side in the eutectic reaction, liquid = Bi_2Te_3 + Te, at 686 K (413 °C), which is lower than 694 K (421 °C). Thus, the temperature-descending direction of the $Bi_2(Se,Te)_3$/(Se,Te) univariant line near the Bi-Te binary side should move toward the Bi-Te side. Therefore, there is a saddle point along the $Bi_2(Se,Te)_3$/(Se,Te) univariant which divides the temperature-descending directions into two different directions.

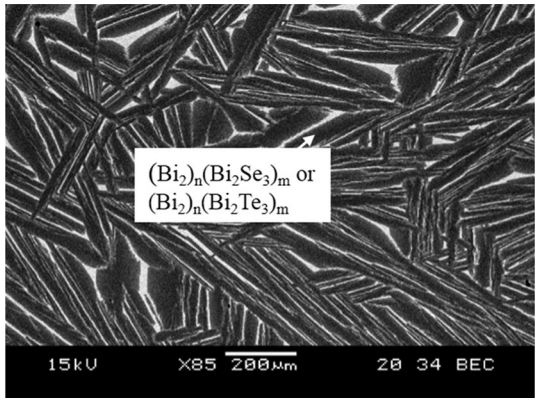

Fig. 11—BEI micrograph of the as-solidified alloy #20 (Bi-5.0 at. pct Se-40.0 at. pct Te) displaying $(Bi_2)_n(Bi_2Se_3)_m$ or $(Bi_2)_n(Bi_2Te_3)_m$ as its primary solidification phase.

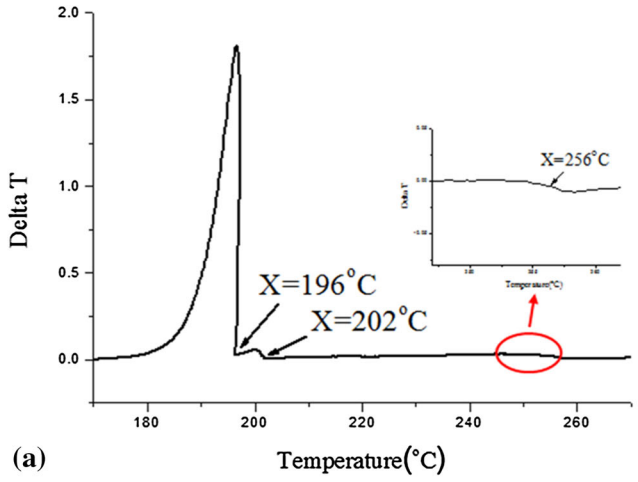

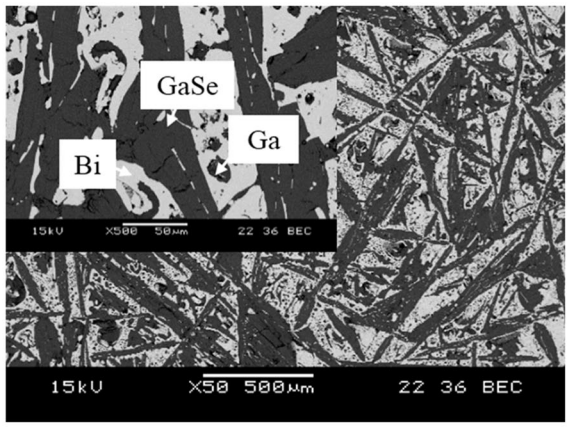

Fig. 12—(*a*) DTA cooling curve of alloy #11 (Bi-20.0 at. pct Se-60.0 at. pct Ga) and (*b*) BEI micrograph of the as-solidified alloy #11.

Table III. Ternary Invariant Reactions in the Bi-Se-Ga System

Type	Reaction	Temperature K(°C)
Class III	Liquid + Bi + GaSe = Ga	495 K (222 °C)
Class II	Liquid + Ga_2Se_3 = GaSe + Bi	533 K (260 °C)

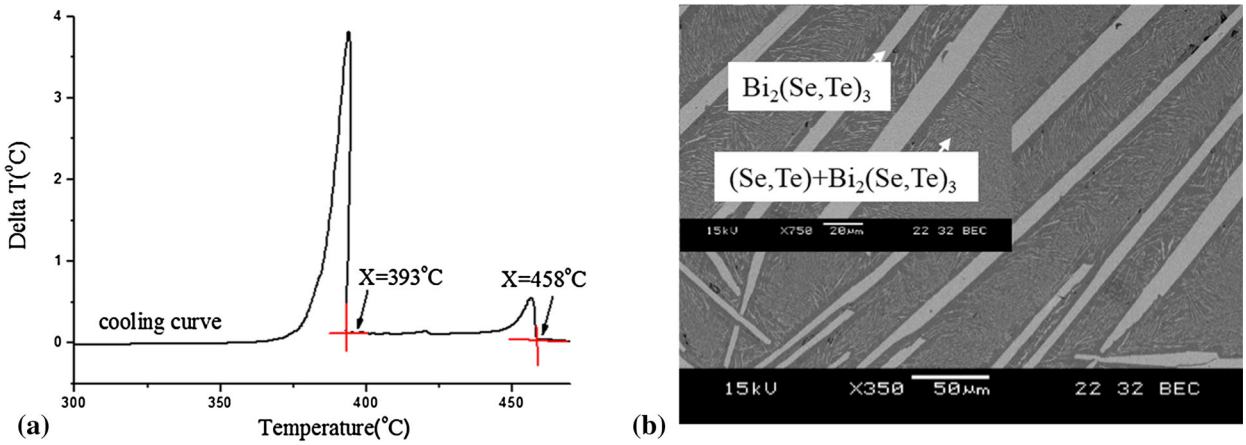

Fig. 13—(*a*) DTA cooling curve of alloy #15 (Bi-10.0 at. pct Se-77.0 at. pct Te) and (*b*) BEI micrograph of the as-solidified alloy #15.

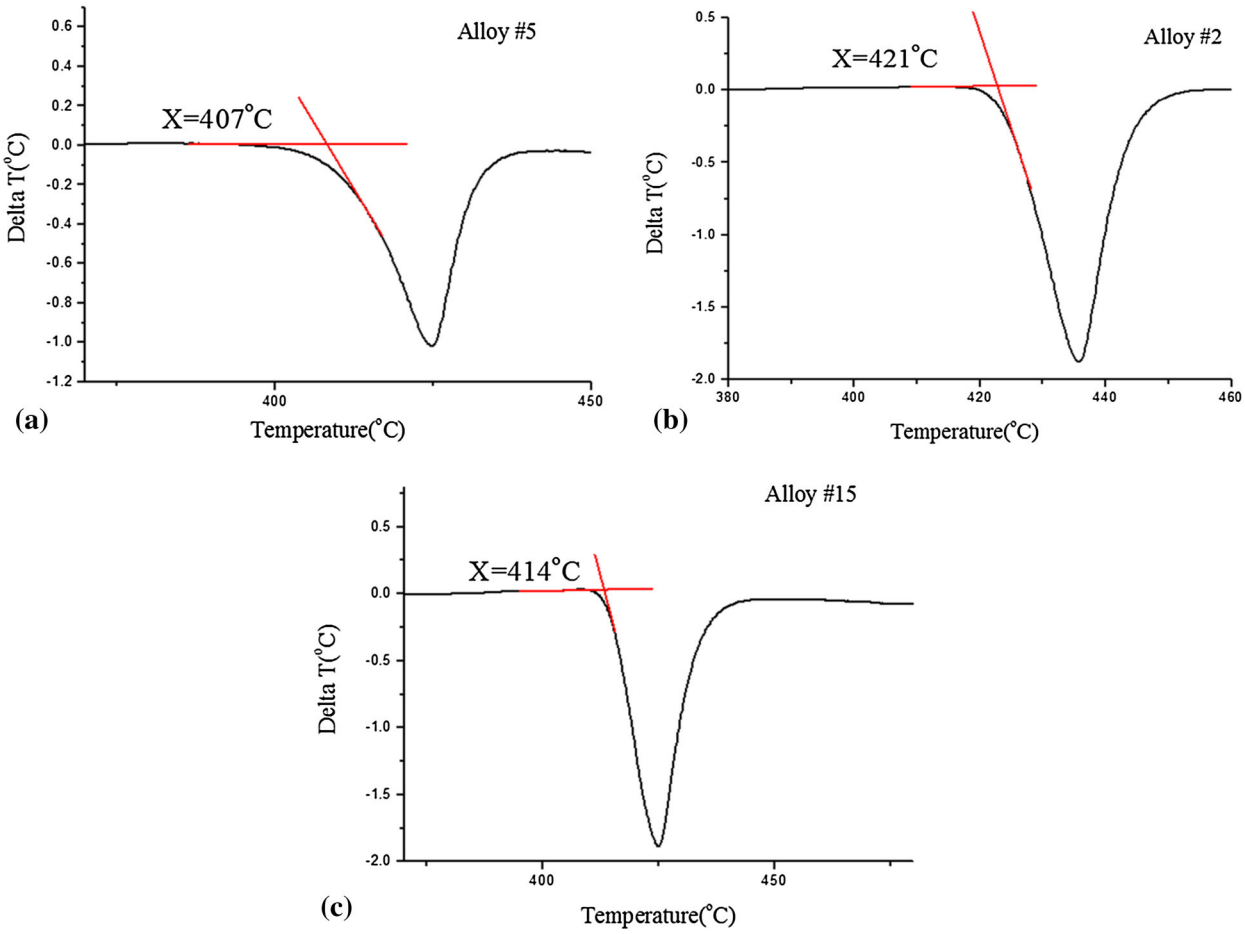

Fig. 14—(*a*) DTA heating curve of alloy #5 (Bi-20.0 at. pct Se-70.0 at. pct Te), (*b*) DTA heating curve of alloy #2 (Bi-5.0 at. pct Se-90.0 at. pct Te), and (*c*) DTA heating curve of alloy #15 (Bi-10.0 at. pct Se-77.0 at. pct Te).

IV. CONCLUSIONS

This study has identified the liquidus projections of both Bi-Se-Ga and Bi-Se-Te. The complicated and undermined series of phases between Bi and Bi_2Se_3 in the Bi-Se system and those between Bi and Bi_2Te_3 in the Bi-Te system are grouped together as the $(Bi_2)_n(Bi_2Se_3)_m$ and $(Bi_2)_n(Bi_2Te_3)_m$ phases, respectively. There are seven primary solidification phases, Bi, Ga, GaSe, Ga_2Se_3, Se, Bi_2Se_3, and $(Bi_2)_n(Bi_2Se_3)_m$, in the Bi-Se-Ga system and five primary solidification phases, Bi, $(Bi_2)_n(Bi_2Te_3)_m$, $Bi_2(Se,Te)_3$, (Se,Te), and $(Bi_2)_n(Bi_2Se_3)_m$ in the Bi-Se-Te system. Very large miscibility gaps are observed in the Bi-Se-Ga system.

ACKNOWLEDGMENTS

The authors acknowledge the financial support of the Materials & Chemical Research Laboratories of ITRI and the Ministry of Science and Technology in Taiwan (NSC103-2923-E-007-002-MY2).

REFERENCES

1. W. Liu, X. Yan, G. Chen, and Z. Ren: *Nano Energy*, 2015, vol. 1, pp. 42–56.
2. G.J. Snyder and E.S. Toberer: *Nat. Mater.*, 2008, vol. 7, pp. 105–14.
3. L.W. da Silva and M. Kaviany: *Int. J. Heat Mass Trans.*, 2004, vol. 47, pp. 2417–35.
4. G. Chen, M.S. Dresselhaus, G. Dresselhaus, J.P. Fleurial, and T. Calliat: *Int. Mater. Rev.*, 2003, vol. 48 (1), pp. 45–66.
5. S.W. Chen, C.Y. Wu, H.J. Wu, and W.-T. Chiu: *J. Alloy. Compd.*, 2014, vol. 611, pp. 313–18.
6. F.J. Manjon, R. Vilaplana, O. Gomis, E. Perez-Gonzalez, D. Santamarıa-Perez, V. Marın-Borras, A. Segura, J. Gonzalez, P. Rodrıguez-Hernandez, A. Munoz, C. Drasar, V. Kucek, and V. Munoz-Sanjose: *Phys. Status Solidi. B*, 2013, vol. 250 (4), pp. 669–76.
7. S.W. Chen, H.J. Wu, C.Y. Wu, C.F. Chang, and C.Y. Chen: *J. Alloy. Compd.*, 2013, vol. 553, pp. 106–12.
8. Y. Ma, W. Wijesekara, and A.E.C. Palmqvist: *J. Electron Mater.*, 2012, vol. 41 (6), pp. 1138–46.
9. Y. Du, K.F. Cai, H. Li, and B.J. An: *J. Electron Mater.*, 2011, vol. 40 (5), pp. 518–22.
10. N. Keawprak, S. Lao-ubol, C. Eamchotchawalit, and Z.M. Sun: *J. Alloy. Compd.*, 2011, vol. 509, pp. 9296–9301.
11. X. Duan, K. Hu, S. Ding, D. Man, and H. Jin: *Prog. Nat. Sci.*, 2015, vol. 25, pp. 29–33.
12. V. A. Kulbachinskii, V. G. Kytin, A. A. Kudryashov, and P. M. Tarasov: *9th European Conference on Thermoelectrics*, *AIP Conf. Proc.*, vol. 1449, pp. 119–22, 2012.
13. D. Zhao, M. Zuo, and H. Geng: *Intermetallics*, 2012, vol. 31, pp. 321–24.
14. V. A. Kulbachinskii, A. V. G. Kytin, and P. M. Tarasov: *International Conference on Thermoelectrics, IEEE proceedings*, pp. 459–64, 2006.
15. C.H. Liu, H.J. Wu, and S.W. Chen: *Metall. Mater. Trans. A*, 2013, vol. 44A, pp. 5424–33.
16. T. Caillat, M. Carle, D. Perrin, H. Scherrer, and S. Scherrer: *J. Phys. Chem. Solids*, 1992, vol. 53 (2), pp. 227–32.
17. M.G. Shakhbazov, N.A. Seidova, and P.G. Rustamov: *Russ. J. Inorg. Chem.*, 1977, vol. 22 (9), pp. 1377–81.
18. P.G. Rustamov, N.A. Seidova, and M.G. Shakhbazov: *Russ. J. Inorg. Chem.*, 1976, vol. 21 (9), pp. 412–15.
19. K. Dobletov, N.K. Samakhotina, A.V. Anikin, and A. Ashirov: *Inorg. Mater.*, 1975, vol. 11, pp. 1036–38.
20. H.G. Bouanani, D. Eddike, B. Liautard, and G. Brun: *Mater. Res. Bull.*, 1996, vol. 31, pp. 177–87.
21. V.F. Bankina and N.K. Abrikosov: *J. Inorg. Chem.*, 1964, vol. 9, pp. 509–12.
22. J.P. McHugh and W.A. Tiller: *Trans. Metall. Soc. AIME*, 1959, vol. 215, pp. 651–55.
23. J.F. Dumas, G. Brun, B. Liautard, J.C. Tédenac, and M. Maurin: *Thermochim. Acta*, 1987, vol. 122, pp. 135–41.
24. R. Eholié and J. Flahaut: *Bull. Soc. Chim. FR.*, 1972, vol. 4, pp. 1250–54.
25. P. G. Rustamov, N. A. Seidova. (1968). *Azerbaidzhanskii Khimicheskii Zhurnal*, 77–80.
26. H. Okamoto: *Binary Alloy Phase Diagrams, 2nd edition*, ASM International, Materials Park, 1990, vol. 1, pp. 738–39.
27. H. Okamoto: *Binary Alloy Phase Diagrams, 2nd edition*, ASM International, Materials Park, 1990, vol. 2, pp. 1852–54.
28. H. Okamoto: *Binary Alloy Phase Diagrams, 2nd edition*, ASM International, Materials Park, 1990, vol. 2, pp. 790–92.
29. J.J. Zhang and G.Q. Huang: *Solid State Commun.*, 2014, vol. 197, pp. 34–39.
30. H. Okamoto and L.E. Tanner: *Binary Alloy Phase Diagrams, 2nd edition*, ASM International, Materials Park, 1990, vol. 1, pp. 800–01.
31. I. Ohnuma, T. Saegusa, Y. Takaku, C.P. Wang, X.J. Liu, R Kainuma, and K Ishida: *J. Electron Mater.*, 2009, vol. 38 (1), pp. 2–9.
32. G. Ghosh, R.C. Sharma, D.T. Li, and Y.A. Chang: *J. Phase Equilib.*, 1994, vol. 15 (2), pp. 213–24.
33. J.W.G. Bos, F. Faucheux, R.A. Downie, and A. Marcinkova: *J. Solid State Chem.*, 2012, vol. 193, pp. 13–18.
34. H.J. Wu and S.W. Chen: *J. Alloy. Compd.*, 2011, vol. 509, pp. 656–58.
35. S.W. Chen and H.J. Wu: *J. Alloy. Compd.*, 2010, vol. 497, pp. 110–17.